Automated Analysis Method for Screening Knee Osteoarthritis using Medical Infrared Thermography

Chao Jin[1] Yang Yang[2] Zu-Jun Xue[3] Ke-Min Liu[3] Jing Liu[1,2,*]

[1]*Department of Biomedical Engineering, School of Medicine, Tsinghua University, Beijing 100084, P. R. China*
[2]*Key Laboratory of Cryogenics, Technical Institute of Physics and Chemistry, Chinese Academy of Sciences, Beijing 100190, P. R. China*
[3]*Department of Orthopedics, Beijing Charity Hospital, School of Rehabilitation Medicine, Capital Medical University, Beijing 100068, P. R. China*

Received 31 Oct 2011; Accepted 21 Feb 2012; doi: 10.5405/jmbe.1054

Abstract

Osteoarthritis (OA) is a major global health issue due to aging populations. Infrared thermography provides functional information on thermal and vascular conditions of knee joints and can thus be used for knee OA screening. However, the thermal diagnostic procedure for various diseases often requires manual analysis and interpretation, which heavily depends on a clinician's personal experience. In this paper, an automated infrared thermographic analysis method for knee OA screening is developed based on the collected data of normal subjects and outpatients in clinics. 266 knee thermal images (166 normal, 100 abnormal) acquired in the China Rehabilitation Research Centre, Beijing, are used for the first trial. An effective knee feature extraction algorithm based on patella-centering is proposed. The extracted features are fed to a support vector machine (SVM) classifier to perform automated recognition. Experimental results indicate that the SVM classifier has an accuracy rate of 85.49%, a sensitivity of 85.72%, and a specificity of 85.51% in detecting normal and abnormal cases. The proposed automated system for knee thermal screening can thus provide quantitative reference information in assisting clinical diagnosis.

Keywords: Automated detection, Infrared thermography, Osteoarthritis screening

1. Introduction

Osteoarthritis (OA) affects over 20 million people in the United States [1]. It is a degenerative disease and one of the most common causes of pain, loss of function, and disability [1]. Early detection or screening of OA allows individual treatment and prevention. OA is commonly characterized using radiography, which indicates anatomical structural changes, such as osteophyte appearance, joint space narrowing, and joint erosion and distortion [1,2]. However, it lacks sufficient sensitivity for the detection of early disease. In order to explore significant diagnostic criteria for the early detection or screening of OA, a growing number of studies have focused on some early symptoms of OA, such as pain symptoms, muscle weakness, and synovitis, which have augmented the physiopathologic knowledge of OA [3,4].

Infrared (IR) thermography provides information on the thermal, metabolic, and vascular conditions of the human body which could be used to interpret the pathophysiologic information related to physical conditions. Studies and clinical observations have proven that IR thermography is a suitable indicator for distinguishing normal and abnormal physiologic progresses, particularly for diseases in their early phase. Furthermore, IR thermography is regarded as a gold standard for breast cancer detection, and is especially applicable to female breast screening due to its unique advantages such as being non-contact and non-invasive and using non-ionizing radiation [5-7].

Several thermographic studies have been performed to assess a series of joint diseases, such as rheumatic disease and OA [8-11]. Some studies have reported that the skin surface temperature at the joint varies with arthritis activity and Kellgren-Lawrence grades of radiographic OA; and a certain correlation between the temperature and arthritis activity has also been established [12,13]. However, no studies have been carried out on estimating the early symptoms of OA using IR thermography.

Most IR thermal diagnosis in clinics require manual analysis and interpretation, which is greatly affected by the experience of clinicians [14]. Computer-aided diagnosis (CAD) techniques have undergone extraordinary development and now play a significant role in medical fields. The application of CAD technology to IR thermal diagnosis is desirable. Some studies have utilized the CAD and pattern recognition technologies to obtain more objective and quantitative thermal diagnosis information, such as the asymmetric analytic method for female breasts, wavelet descriptor and fractal descriptor of

* Corresponding author: Jing Liu
Tel: +86-10-62794896; Fax: +86-10-82543767
E-mail: jliubme@tsinghua.edu.cn

localized thermal distributions of tumors, and advanced classification approaches [15-23]. Most of these efforts have focused on the automated IR thermal diagnosis for breast cancer, with few trials conducted for OA diagnosis.

In our previous study, a thermal screening method based on patella-centering was proposed for knee OA screening. An average screening accuracy rate of 91.558% ($p < 0.05$) and a sensitivity of 93.5% were obtained in distinguishing normal and abnormal cases. This paper conducts a preliminary study on an automated thermographic analysis for knee OA screening. A feature extraction method based on patella-centering is proposed and a support vector machine (SVM) classifier is adopted to validate its effectiveness. The proposed automated screening system can improve the efficiency of clinicians by providing more quantitative and convenient diagnostic references of knee OA. Additionally, this work advances the standardization of medical IR imaging diagnosis and offers numerous knee cases for the construction of a medical imaging database.

2. Materials and methods

2.1 Subjects

177 subjects were recruited (July 2010 to December 2010) for the clinical experiments in the China Rehabilitation Research Centre (CRRC). Subjects were excluded if they had a clinical diagnosis or radiographic evidence of joint disease due to trauma on the knee joint, or a definite clinical diagnosis of OA. 133 subjects were selected to participate in this study.

Pain is considered a typical early feature of knee OA in clinics. Thus, subjects who had a history of knee joint pain evaluated by the clinical index WOMAC (Western Ontario and McMaster Universities) were assigned to the abnormal group and those who had no pain were assigned to the normal group [24]. 83 healthy subjects were included in the normal group and 50 outpatients were assigned to the abnormal group. Informed consent was obtained from all subjects and approval was obtained from CRRC's institutional review board.

2.2 Knee thermography data acquisition

2.2.1 Thermal measurement system

IR thermograms of knees were acquired using an IR thermal imaging system (FLIR SC620, FLIR Systems Inc, USA). An ambient temperature of 25 ℃ ± 1℃ and a constant humidity of 50% ± 10% were maintained in a standardized control room, in which a micro-diameter hole was utilized for the air supply to avoid the effect of wind on human skin surface temperature.

2.2.2 Knee joint positioning in thermal measurement procedure

For standardized knee thermographic analysis, a human knee positioning criteria was established prior to each subject's thermographic test. As shown in Fig. 1(a), the knee positioning device consisted of a vertical support bar and two horizontal boundary markers. The lower boundary of the knee positioning device was located at the tibial tubercle and the coboundary was 5 cm up along the patella.

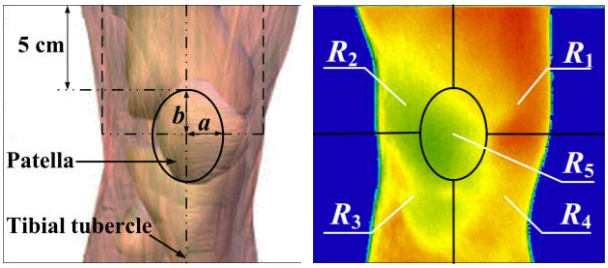

(a) (b)

Figure 1. Knee anatomy structure and schematic diagram of subregion segmentation based on patella-centering. (a) Location of knee joint, including tibial tubercle and the site 5 cm along the patella; (b) thermographic image of subregions of knee joint, where R_5 represents the patella region and R_1, R_2, R_3, and R_4 denote the other regions of the knee.

2.2.3 Infrared imaging procedure for the knee joint

Before the IR thermographic examination, subjects were seated with their legs uncovered for 10 minutes, which regulated the knee joint to a relatively steady state via the thermal physiological regulation system.

During the process of thermal examination, the distance between the subject and the camera was maintained at 2 m. IR thermograms were captured on the anterior, posterior, extra-lateral, and medial-lateral sides of the knees in turn. At the beginning of the experiment, it was necessary to evaluate the reliability of the imaging technique.

2.3 Patella-centering diagnostic criteria for OA early screening

Conventional medical imaging methods such as X-ray, computed tomography, and magnetic resonance imaging indicate anatomical changes in the knee for assessing the severity of OA. Thermographic research has explored the correlation between the skin surface temperature on the knee patella and X-ray severity of knee OA [13]. Our previous work provided valuable thermal-physiological information for evaluating the early development of OA, especially for early pain, which is commonly assessed using the WOMAC index in clinics. Based on knee surface anatomy and a clinical symmetry analysis of thermal pattern distribution, a semi-automated diagnostic method based on patella-centering was developed. As shown in Fig. 1(b), the knee joint is segmented into five regions, namely R_1, R_2, R_3, R_4, and patella region R_5. Patella region R_5 is specified as an ellipse with semi-axes a and b whose center is in the middle point of the knee region. Semi-axes a and b were one sixth of the width and height of the knee region, respectively. The width of the knee region was determined by two points that denoted respectively left and right intersections between the horizontal center line and the left and right edges of the knee. The above measurements depend on the knee anatomy.

The preliminary results indicated that in the normal group, subregions R_1~R_4 had a higher temperature than that of region R_5. The difference between subregions R_1~R_4 and region R_5 was lower in the abnormal group. Based on these findings, the patella-centering diagnostic method consisted of two

procedures. In the first step, a symmetric comparison is conducted between the left and right knees. In the second step, the temperature difference between subregions R_1~R_4 and region R_5 is determined. An ultimate screening accuracy of 91.558% ($p < 0.05$) and a sensitivity of 93.5% verify the feasibility and efficiency of the proposed method in assessing knee thermal images.

2.4 Automated thermal method for knee OA

This study conducts a preliminary study on an automated thermal screening system for knee OA. As shown in Fig. 2, the system has four major procedures: (a) segmentation of the thermal image into the left and right knees; (b) subregional segmentation based on patella-centering; (c) feature extraction; (d) SVM classification.

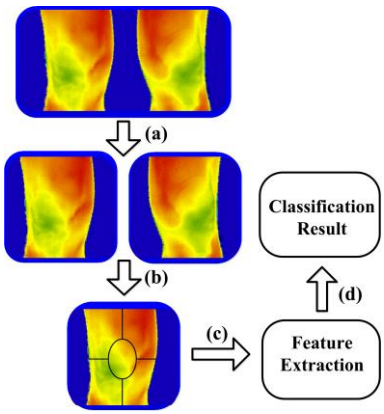

Figure 2. Schematic diagram of the proposed automated thermal analysis procedure for knee OA screening. (a) Segmentation of thermal image between left and right knees; (b) subregional segmentation based on patella-centering; (c) feature extraction; (d) automated classification.

2.4.1 Method for processing knee thermography images

In the automated thermal screening system, each region is defined by the boolen identification function BI_l : {*all pixels*} →[0,1], (l = 1, 2, 3, 4, 5). The function BI_5 for region R_5 can be expressed as $\mathrm{BI}_5(x, y) = 1$ when (x, y) is in E_{ab}; otherwise $\mathrm{BI}_5(x,y) = 0$. Here, (x, y) denotes the position of a pixel or a temperature value in the thermal image and (x_0, y_0) is the E_{ab} centre. Then, the function $\mathrm{BI}_1(x, y)$ for region R_1 can be computed as $(1 – \mathrm{BI}_5(x, y))$ when $x > x_0$ and $y > y_0$; otherwise $\mathrm{BI}_1(x, y) = 0$. Other regions including R_1~ R_4 are determined by the obvious reflections because of their symmetrical relations in the Cartesian coordinate system.

After the function BI_l has been obtained, the five regions can be segmented simply using matrix multiplication as $I_l = \mathrm{BI}_l \times I$, where I_l denotes the target region temperature mapping and I denotes the original thermal image.

2.4.2 Knee thermography image feature extraction

Statistical features are extracted from subregions R_1~ R_5 to distinguish normal and abnormal cases.

Mean and standard deviation of temperature distribution: In clinical practice, the mean temperature is a crucial physiological parameter in localized areas for thermal diagnosis. The standard deviation can be adopted as a measurement of thermal distribution uniformity. Therefore, the means and standard deviations of subregions R_1~R_5 are calculated using Eq. (1) and Eq. (2), respectively. According to the thermal screening method based on patella-centering, the four mean temperature differences between R_1, R_2, R_3, R_4, and patella region R_5 are adopted as the first feature vector components. The five standard deviations are listed in the second feature vector.

$$T_{mean} = \frac{1}{M \cdot N} \sum_{j=0}^{N-1} \sum_{i=0}^{M-1} T_{ij} \tag{1}$$

$$\sigma_{std}^2 = \frac{1}{M \cdot N} \sum_{j=0}^{N-1} \sum_{i=0}^{M-1} (T_{ij} - T_{mean})^2 \tag{2}$$

where T_{mean} and σ_{std} denote the mean temperature and standard deviation, respectively. T_{ij} and $M \cdot N$ present the temperature pixel and the size of each thermal image, respectively.

Calculation of histogram features: As a statistical measurement, the histogram of a thermal image is a discrete function $h(T_k) = n_k$, where T_k is the kth temperature level and n_k is the number of pixels in the image with temperature level T_k [25]. A normalized histogram can be calculated as $p_l(T_k) = n_k / n$ ($l = 1, \cdots, 5$; $k = 0, 1, \cdots, L-1$), where n denotes the total number of pixels in the image. L is determined from the temperature scale and the thermography resolution of the IR camera; it is set as 256 in this paper (temperature scale 28~36℃; FLIR SC620 camera, sensitivity of 0.065℃). The normalized histogram difference distribution was obtained by subtracting $p_5(T_k)$ from $p_l(T_k)$ (l = 1,2,3,4). Therefore the normalized histogram difference distribution of subregion R_1 can be expressed as:

$$p_{\Delta 1}(T_k) = p_1(T_k) - p_5(T_k) \tag{3}$$

For a normal subject, the normalized histogram difference distribution between subregions R_1~R_4 and patella region R_5 is shown in Fig. 3. The horizontal axis represents the temperature

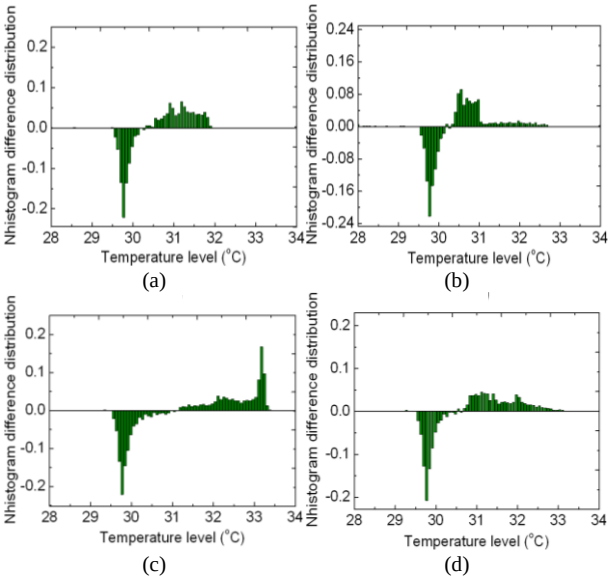

Figure 3. Normalized histogram difference distribution of a normal subject case. Normalized histogram difference distributions of (a) (R_1-R_5), (b) (R_2-R_5), (c) (R_3-R_5), and (d) (R_4-R_5). Here, Nhistogram represents the normalized histogram.

level values and the vertical axis corresponds to the difference of normalized histograms. The negative components of the histogram are distributed in the low value part of the temperature level axis and the positive components are distributed in the high value part For the abnormal case, shown in Fig. 4, the negative components are distributed in the high value part of the temperature level axis and the positive components are distributed in the low value part.

Based on the above results, a series of useful image statistical characteristics for distinguishing normal and abnormal cases was extracted. For each normalized histogram difference distribution, the distance between the maximum and minimum energy magnitudes is computed. The counts of temperature levels and the total energy in the negative part and the positive part are calculated, respectively. Thus, five features, namely two counts, two energy magnitudes, and a distance measurement, in each normalized histogram difference distribution are obtained. The third feature vector has 20 features.

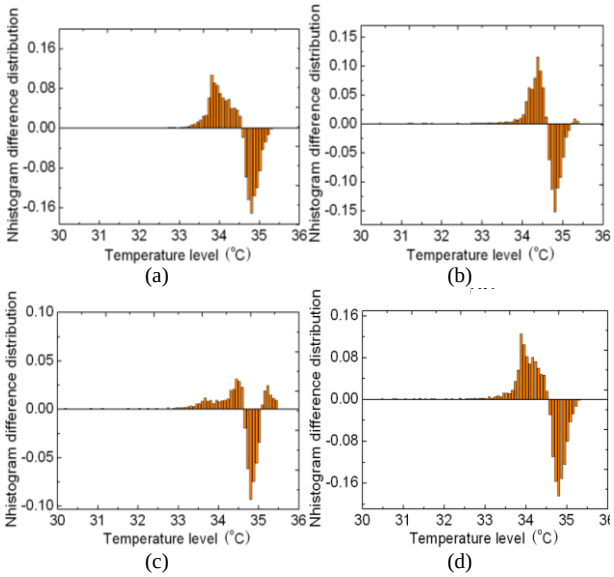

Figure 4. Normalized histogram difference distribution of an abnormal subject case. Normalized histogram difference distributions of (a) (R_1-R_5), (b) (R_2-R_5), (c) (R_3-R_5), and (d) (R_4-R_5). Here, Nhistogram represents the normalized histogram.

Calculation of entropy features: The information entropy features of the five subregions are employed as signal characteristics [26].

$$H(R_l) = -\sum_{k=0}^{L-1} p(T_k)\log\ p(T_k) \tag{4}$$

where R_l denotes the subregion segmented from the original knee thermal image and T_k is the kth temperature level. The entropy features normalized to the interval [0:1] are:

$$H\ (R_l\ ) = \frac{H\ (R_l)}{\sum H\ (R_l)} \tag{5}$$

The fourth feature vector has five normalized entropy features. As listed in Table 1, 34 features in four feature vectors can be extracted from each knee thermography image for determining the differences between R_1, R_2, R_3, R_4, and patella region R_5. A large feature dataset of 266 images was created after the feature extraction operation. In addition, the multivariate analysis of variance (MANOVA) test results ($p < 0.05$) verify the efficiency of this feature approach in differentiating normal and abnormal knee joints.

Table 1. Feature vectors extracted from each knee thermal image.

Feature Vector	Vector Elements
Vector1	($\Delta T_{mean(1\text{-}5)}$, $\Delta T_{mean(2\text{-}5)}$, $\Delta T_{mean(3\text{-}5)}$, $\Delta T_{mean(4\text{-}5)}$)
Vector2	(σ_{std1}, σ_{std2}, σ_{std3}, σ_{std4}, σ_{std5})
Vector3	($N_{p(1\text{-}5)}$, $N_{n(1\text{-}5)}$, $E_{p(1\text{-}5)}$, $E_{n(1\text{-}5)}$, $d_{1\text{-}5}$) ($N_{p(2\text{-}5)}$, $N_{n(2\text{-}5)}$, $E_{p(2\text{-}5)}$, $E_{n(2\text{-}5)}$, $d_{2\text{-}5}$) ($N_{p(3\text{-}5)}$, $N_{n(3\text{-}5)}$, $E_{p(3\text{-}5)}$, $E_{n(3\text{-}5)}$, $d_{3\text{-}5}$) ($N_{p(4\text{-}5)}$, $N_{n(4\text{-}5)}$, $E_{p(4\text{-}5)}$, $E_{n(4\text{-}5)}$, $d_{4\text{-}5}$)
Vector4	(H_1, H_2, H_3, H_4, H_5)

$\Delta T_{mean(i\text{-}5)}$ denotes the mean temperature difference between subregions R_i and R_5; σ_{stdj} represents the standard deviation in each subregions R_j ;
$N_{p(i\text{-}5)}$ and $N_{n(i\text{-}5)}$ denote the counts of temperature levels in positive part and negative part, respectively; $E_{p(i\text{-}5)}$ and $E_{n(i\text{-}5)}$ indicate the total energy in negative part and positive part, respectively; $d_{i\text{-}5}$ is the distance between the maximum and minimum energy magnitudes;
H_j indicates the normalized entropy feature in each subregion;
i = 1,2,3,4 and j = 1,2,3,4,5.

2.4.3 Classification method

Among the classification methods available for solving pattern recognition problems, the SVM classifier has been proven to be an efficient way of obtaining good classification performance [27]. Therefore, the features extracted are fed to the SVM classifier to develop an automated diagnostic method for knee OA.

As shown in Fig. 5, the process of SVM classification involves two primary procedures, namely those of training and testing. Based on the training dataset (feature vector and class label contained in each dataset), the goal of the SVM classifier is to produce a decision model that can predict the class label of the test data given only the feature vector. The key of the SVM algorithm is to solve the following optimization problem [27]:

$$\min\ \frac{1}{2}\ w^T w + C\sum_{i=1}^{l}\ \xi_i$$

$$\text{subject to}\ \ y_i\ (w^T\varphi(x_i) + \ b) \geq 1 - \xi_{\ i} \tag{6}$$

$$\xi_{\ i}\ \geq 0,\ i = 1,\ldots,l$$

where x_i and y_i ($i = 1,\ldots,l$) denote the training feature vector and corresponding class label, respectively. The training feature vector x_i is mapped into a higher dimensional space by the function $\varphi(x_i)$ and $C > 0$ is the regularization parameter. $K(x_i,x_j) = \varphi^T(x_i)\varphi(x_j)$is called the kernel function.

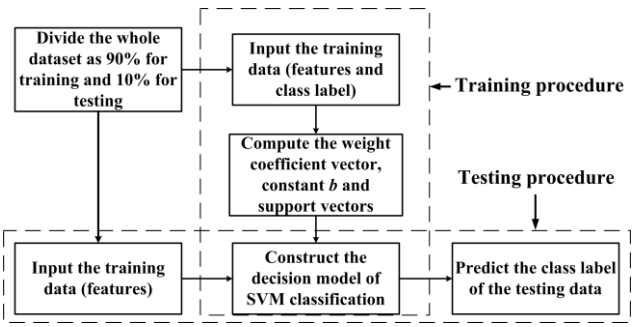

Figure 5. Flow chart of SVM classification process.

After problem (6) is solved, the decision model of the SVM classifier can be constructed as:

$$y = \text{sgn}\ (\sum_{i=1}^{d} \alpha_i y_i K(x_i, x_j) + b) \quad (7)$$

where $x = (x_1, x_2, \cdots, x_d)$ is the input testing data, $w = \{w_1, w_2, \cdots, w_s\}$ is the vector of coefficients, where $w_i = \alpha_i y_i$, b is a constant, and $y = \{+1, -1\}$ is the predicted class label. The decision model is used to predict the class label of the input testing data.

3. Results

3.1 Classification results

In the classification experiment, the feature datasets were divided into training and testing datasets. The former were used to build the classifier and the latter were used to evaluate the classifier. In addition, 10-fold cross-validation on the feature dataset was performed. The feature datasets were divided into 10 subsets. In each test, one feature dataset was used as the testing dataset, and the remaining nine datasets were employed to train the classifier. In each test, the true positives (*TP*s), true negatives (*TN*s), false positives (*FP*s), and false negatives (*FN*s) of the testing dataset were recorded after comparing the predicted and actual class labels. Based on the predicted results, a series of crucial indices for evaluating the efficiency of the proposed method are obtained. They are classification rate (accuracy) = $(TP + TN)/(TP + TN + FP + FN)$, sensitivity = $TP/(TP + FN)$, specificity = $TN/(TN + FP)$, positive predictive value (PPV) = $TP/(TP + FP)$, and negative predictive value = $TN/(TN + FN)$. After the 10-fold cross- validation tests, the average results were computed. Table 2 lists statistical analysis results and Table 3 lists the average results of SVM classification.

Table 2. Statistical analysis results of 10-fold cross-validation test.

TN	*TP*	*FN*	*FP*
15.8 ± 1.13	7.4 ± 2.01	1.2 ± 1.13	2.6 ± 2.01

The statistical analysis results of 10-fold cross-validation test are presented as mean ± SD; in each test, the numbers of normal and abnormal cases were 17 and 10, respectively.

Table 3. Results of SVM classification.

Classification rate (%)	Sensitivity (%)	Specificity (%)	Positive predictive value (%)	Negative predictive value (%)
85.49%	85.72%	85.51%	73%	92.94%

3.2 Implementation of automated thermal screening system

The proposed automated system for knee thermal screening was implemented. Figure 6 shows a flow chart of the system, whose main processes are the input of a test knee thermal image, left and right knee segmentation, and classification processing. The pre-processing procedure removes background noise based on a threshold denoising strategy. An edge detection algorithm then segments the left and right knee joints from the original image. During SVM classification, subregions R_1~R_5 are segmented in the left or right knee thermal image, as detailed in Section 2.4.1. 34 features are extracted according to the feature extraction method described in Section 2.4.2. In the final step, the preliminary SVM classifier is constructed by the training dataset, which consists of the feature datasets extracted from the 266 images. The features extracted from the input image are utilized as the testing dataset to predict the class label (normal or abnormal).

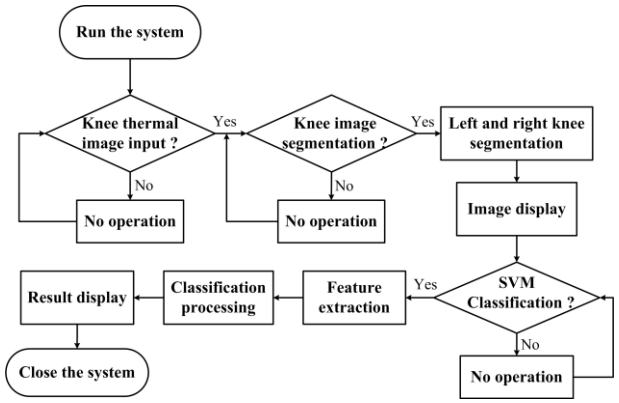

Figure 6. Flow chart of automated thermal screening system.

A snapshot of the graphical user interface developed for the proposed system is shown in Fig. 7. The *Open* button brings

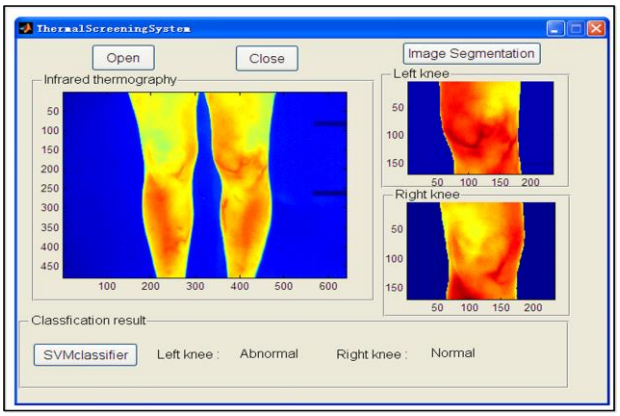

(a)

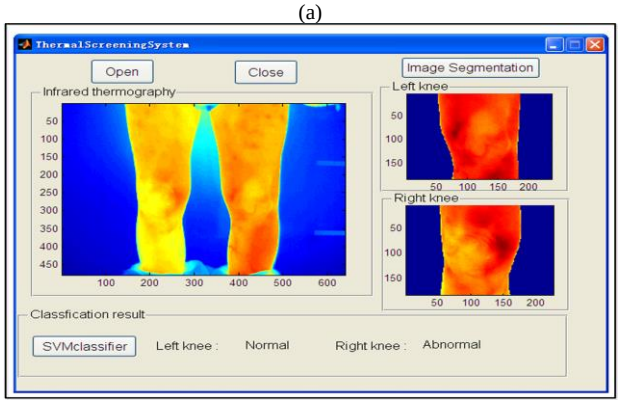

(b)

Figure 7. Graphical user interface of automated thermal screening system. (a) Screening result of a female subject (70 years old, BMI = 23.31, a history of left knee pain for more than 2 months); (b) screening result of a male subject (75 years old, BMI = 23.58, a history of right knee pain for about half a year) (BMI denotes Body Mass Index).

up a dialog to load a test knee thermal image. The *Image Segmentation* button is used to segment the left and right knees from the selected image. The *SVMclassifie*r button is used to automatically extract features from the left and right knee thermal images. These features are then fed into the SVM classifier to identify the class label. The classification results are exported and displayed in section 3.1. The screening results of female and male subjects (not included in the 266 images) are shown in Figs. 7(a) and 7(b), respectively. For the female, the left and right knees are determined as abnormal and normal, respectively, by the SVM classifier. For the male, the left and right knees are normal and abnormal, respectively.

4. Discussion

In our previous work, a patella-centering subregional analytic criterion for OA was developed by using IR thermography to characterize the thermal pattern differences between normal and abnormal knee joint cases. Based on this approach, the present study proposed a thermal image feature extraction algorithm for translating the thermal pattern differences between subregions R_1, R_2, R_3, R_4, and patella region R_5 into a series of feature vectors for the mean temperature difference, standard deviation, normalized histogram distribution differences, and information entropy. The mean temperature difference is a critical physiological parameter for the thermal diagnosis of various diseases. The standard deviation in each sub-region can be adopted as a measurement of thermal distribution uniformity, which has good sensitivity for capturing localized disease changes. The features extracted from the normalized histogram difference can be utilized to characterize the comparisons of the statistical measurement of the temperature level, which exhibit distinct changes due to the occurrence of disease. In the normal cases, the negative components were distributed in the low value part of temperature level axis and the positive components were distributed in the high value part, and vice versa for the abnormal cases. The normalized entropy feature in each sub-region is an uncertainty measurement which represents the probability descriptors of temperature mapping. The SVM method achieved a classification rate of 85.49%, a sensitivity of 85.72%, and a specificity of 85.51% (shown in Table 2). The method has a high negative predictive value and consequently an extremely low omission rate of abnormal cases, which is a significant factor for knee OA screening.

In addition, 10-fold cross-validation tests were performed to explore the contribution of each feature vector (described in Section 2.4.2) in the pattern recognition problems of thermal screening. The results indicate that the feature vector consisting of the temperature mean differences between subregions R_1~R_4 and patella region R_5 had the best classification rate (83.2%). The accuracies for the normalized histogram difference distribution, information entropy feature vector, and standard deviation feature vector were 75.2%, 62.0%, and 62.3% respectively. The classification experiment results demonstrate that the combination of feature vectors gives a high classification rate for the thermal screening of knee OA.

CAD plays an important role in the analysis of IR thermal images, as human examination and interpretation of images are often influenced by factors such as the fatigue, carelessness, and subjectivity of clinicians. Therefore, it is desirable to develop more quantitative methods, such as functional feature indications of thermal images, multimodality imaging fusion, and other advanced pattern classification methods. In medical thermal diagnosis, both the position selection and descriptors of the disease are two critical factors that challenged the clinicians and researches. The thermal diagnosis of breast cancer has seen extraordinary development, with advances such as the asymmetric analytic method, wavelet descriptors, and fractal descriptors [7]. The thermal evaluation of OA, especially for early diagnosis, is still in its infancy. In this work, a convenient and feasible automated system for knee thermal screening or physical examination was implemented to provide quantitative reference information for clinical diagnosis. A good preliminary screening accuracy was obtained.

However, differences in individual anatomical structures and diagnostic mistakes are still challenges for CAD techniques in the field of medical IR thermal imaging. For example, subregional segmentation and leads to some uncertainties in the thermal detection of knee OA due to joint boundary determination and approximate ellipse presentation of the patella region. Therefore, further work should be conducted to guarantee the exact quantitative presentation of individual anatomical locations in a thermal image using techniques such as multi-image fusion with CT and MRI, which would greatly improve the accuracy of the screening procedure. In addition, there are some uncertainties concerning the physiopathological interpretation of the knee joint, such as the relation among inflammation, pain, thermal manifestations, and OA progression. Thus, it is necessary to carry out follow-up clinical tracking of subjects to clarify the mechanisms of OA progression. Although the proposed method cannot replace clinicians, it provides objective and quantitative information.

Although the WOMAC index depends on the subjective scoring of clinicians, it is commonly used to grade the pain of OA. Compared with the WOMAC index, IR thermography provides much more objective and quantitative thermal-physiological information of the knee joint. This functional imaging modality is rather sensitive in detecting human abnormalities in the very early stages. Therefore, this study used IR thermography for the early evaluation of OA. The preliminary results verify the efficiency of the thermal analytic method for knee joints. It is necessary to establish principles for the long-term follow-up of OA progression. Based on the golden standard of OA diagnosis, a more detailed grouping strategy of subjects should be adopted according to the degenerative representations of the knee joint, such as osteophyte appearance, joint space narrowing, and joint erosion.

As a non-invasive, non-contact, and cost-effective functional imaging modality, IR thermal imaging has become a useful tool for the screening of various diseases, especially chronic ones [5-8]. Compared to X-ray, CT, MRI, ultrasonic imaging, and other medical imaging modalities, IR thermal

imaging has distinct advantages in the diagnosis of rheumatism, soft tissue diseases, and other common geriatric sicknesses. Advances in related areas have improved the imaging resolution and temperature sensitivity of IR thermal imaging, which have allowed more applications in medicine. In new diagnostics modality, the knowledge-based medical imaging database system is emerging, which holds the potential of widespread use in sharing various valuable clinical information for disease diagnosis, tele-medicine, scientific research and teaching. The proposed system paves the way for the construction of an expert decision system in the field of disease thermal diagnosis.

5. Conclusion

A convenient and feasible automated system for knee thermal screening was implemented to provide quantitative reference information for clinical diagnosis. An effective knee feature extraction method based on patella-centering was proposed. The features are fed to an SVM classifier for automatic recognition. Experimental results demonstrate that the SVM classifier achieved an accuracy of 85.49%, a sensitivity of 85.72%, and a specificity of 85.51% in detecting normal and abnormal cases. The proposed system is suitable for knee OA screening or physical examination.

Acknowledgements

This work was partially supported by the Handicapped Aided Research Fund from the Chinese Academy of Sciences and the Tsinghua-Yue-Yuen Medical Science Fund.

References

[1] N. Arden and M. C. Nevitt, "Osteoarthritis: epidemiology," *Best Pract. Res. Clin. Rheumatol.*, 20: 3-25, 2006.

[2] J. Sellam and F. Berenbaum, "The role of synovitis in pathophysiology and clinical symptoms of osteoarthritis," *Nat. Rev. Rheumatol.*, 6: 625-635, 2010.

[3] V. Valderrabano and C. Steiger, "Treatment and prevention of osteoarthritis through exercise and sports," *J. Aging Res.*, 2011: 1-6, 2011.

[4] S. Ikeda, H. Tsumura and T. Torisu, "Age-related quadriceps-dominant muscle atropy and incident radiographic knee osteoarthritis," *J. Orthop. Sci.*, 10: 121-126, 2005.

[5] I. Fujimas, "Pathophysiological expression and analysis of far infrared thermal images," *IEEE Eng. Med. Biol. Mag.*, 17: 34-42, 1998.

[6] B. F. Jones, "A reappraisal of the use of infrared thermal image analysis in medicine," *IEEE Trans. Med. Imaging*, 17: 1019-1027, 1998.

[7] E. Y. K. Ng, "A review of thermography as promising non-invasive detection modality for breast tumor," *Int. J. Therm. Sci.*, 48: 849-859, 2009.

[8] C. Hildebrandt, "An overview of recent application of medical infrared thermography in sports medicine in Austria," *Sensors*, 10: 4700-4715, 2010.

[9] R. K. Will, E. F. J. Ring, A. K. Clarke and P. J. Maddison, "Infrared thermography: what is its place in rheumatology in the 1990s ?" *Br. J. Rheumatol.*, 31: 337-344, 1992.

[10] M. Brenner, C. Braun, M. Oster and P. S. Gulko, "Thermal signature analysis as a novel method for evaluating inflammatory arthritis activity," *Ann. Rheum. Dis.*, 65: 306-311, 2006.

[11] M. Frize, J. Karsh, C. Herry, C. Adea, I. Aleem and P. Payeur, "Preliminary results of severity of illness measures of rheumatoid arthritis using infrared imaging," *IEEE Int. Workshop on Medical Measurements and Applications*, 187-192, 2009.

[12] G. Varjú, C. F. Pieper, J. B. Renner and V. B. Kraus, "Assessment of hand osteoarthritis: correlation between thermographic and radiographic methods," *Rheumatology*, 43: 915-919, 2004.

[13] A. E. Denoble, N. Hall, C. F. Pieper and V. B. Kraus, "Pattellar skin surface temperature by thermography reflects knee osteoarthritis severity," *Clin. Med. Insights: Arthritis Musculoskelet. Disord.*, 3: 69-75, 2010.

[14] J. Koay, C. Herry and M. Frize, "Analysis of breast thermography with an artificial neural network," *Conf. Proc. IEEE Eng. Med. Biol. Soc.*, 1: 1159-1162, 2004.

[15] T. Z. Tan, C. Quek, G. S. Ng and E. Y. K. Ng, "A novel cognitive interpretation of breast cancer thermography with complementary learning fuzzy neural memery structure," *Expert Syst. Appl.*, 33: 652-666, 2007.

[16] F. Abu-Amara and I. Abdel-Qader, "Detection of breast cancer using independent component analysis," *IEEE Int. Conf. Electro/Information Technol.*, 428-431, 2007.

[17] C. L. Herry and M. Frize, "Quantitative assessment of pain-related thermal dysfunction through clinical digital infrared thermal imaging," *Biomed. Eng. Online*, 3: 19, 2004.

[18] E. Y. K. Ng and E. C. Kee, "Advanced integrated technique in breast cancer thermography," *J. Med. Eng. Technol.*, 32: 103-114, 2008.

[19] C. S. Yang and M. Y. Lee, "A novel data mining algorithm and knowledge-based diagnostic rules for medical thermography," *Biomed. Eng. App. Bas. C.*, 21: 1-8, 2009.

[20] L. Boquete, S. Ortega, J. M. Miguel-Jiménez, J. M. Rodríguez-Ascariz and R. Blanco, "Automated detection of breast cancer in thermal infrared images based on Independent Component Analysis," *J. Med. Syst.*, 36: 103-111, 2012.

[21] E. Y. K. Ng, S. C. Fok, Y. C. Peh, F. C. Ng and L. S. J. Sim, "Computerized detection of breast cancer with artificial intelligence and thermograms," *J. Med. Eng. Technol.*, 26: 152-157, 2002.

[22] G. Schaefer, M. Závišek and T. Nakashima, "Thermography based breast cancer analysis using statistical features and fuzzy classification," *Pattern Recognit.*, 42: 1133-1137, 2009.

[23] T. Z. Tan, C. Quek, G. S. Ng and E. Y. K. Ng, "A novel cognitive interpretation of breast cancer thermography with complementary learning fuzzy neural memory structure," *Expert Syst. Appl.*, 33: 652-666, 2007.

[24] S. McConnell, P. Kolopack and A. M. Davis, "The Western Ontario and McMaster Universities Osteoarthritis Index (WOMAC): a review of its utility and measurement properties," *Arthritis Rheum.*, 45: 453-461, 2001.

[25] R. C. Gonzalez and R. E. Woods, "Intensity transformation and spatial filtering," in: R. C. Gonzalez and R. E. Woods (Ed.), *Digital image processing*, Beijing: Publishing House of Electronic Industry, 142-143, 2010.

[26] R. C. Gonzalez and R. E. Woods, "Representation and description," in: R. C. Gonzalez and R. E. Woods (Ed.), *Digital image processing*, Beijing: Publishing House of Electronic Industry, 850-851, 2010.

[27] S. Theodoridis and K. Koutroumbas, "Nonlinear classifier," in: S. Theodoridis and K. Koutroumbas, (Ed.), *Pattern recognition*. Canada: Academic Press, 198-203, 2009.